COMPARISON OF THE EMISSIONS OF CURRENT EXPENDABLE LAUNCH VEHICLES AND FUTURE SPACEPLANES

Robert J. Garner*, **Federico Toso**†, **Christie Alisa Maddock**‡
Centre for Future Air Space Transportation Technologies
University of Strathclyde, Scotland, United Kingdom

This paper compares the environmental impact of two types of launch vehicles, an expendable vertical launcher (Delta IV) and an SSTO spaceplane. A realistic trajectory for the spaceplane is generated using a multiple-shooting trajectory optimisation method, which integrates physical models and generates an optimal control law minimising the fuel consumption and the emissions of the flight. These were compared with the emissions from a standard Delta IV trajectory. The launch was to a 200 km circular LEO at 27.5° inclination. The chemical investigated is H_2O, which contributes to the depletion of the ozone layer in the stratosphere. The study shows that for the ascent trajectory the spaceplane produces a total of 5.0143×10^5 kg of H_2O, compared with 2.24×10^5 kg for the Delta IV. The spaceplane has a peak production altitude in the sensitive lower stratosphere, compared to the much lower peak production altitude of the Delta IV.

I INTRODUCTION

Spaceplanes are an aerospace vehicle that are capable of operating as an aircraft, deriving support in the atmosphere from the reaction of the air, and as a rocket-based spacecraft in a vacuum. Subcategories of these vehicle are often based the take-off: horizontal or vertical take-off from the ground, or air-launched systems. It is also possible to introduce staging into these designs, with a lower stage spaceplane bringing the payload to an altitude near or into space, and an expendable upper stage to inject the payload into a higher orbit.

Spaceplanes, and in particular single-stage-to-orbit (SSTO) vehicles, have been proposed as a possible solution to reducing the cost of access to space due in large part to their reusable nature. Recently there has been significant progress in the development of technologies capable of overcoming the major challenges of these vehicles, such as novel propulsion systems[1] and reusable thermal protection systems. In order to fully explore the advantages and disadvantages of spaceplanes compared to expendable launch vehicles, both their performance and operational issues, such as their environmental impact must be investigated.

The current regulatory and political climate places much emphasis on the responsibility of industry and governments to minimise the impact of transportation on the environment. For countries to meet their responsibilities to broad international agreements such as the Kyoto Agreement, significant financial investments have been made in the development of new technologies such as environmentally friendly materials, low-carbon technology and alternative fuels. Examples of this are the EU Clean Sky (1 & 2) Programme and NASA's Advanced Air Vehicles Program. The International Civil Aviation Organization (ICAO) publishes goals and technical standards to manage the impact of aviation on the environment. There have been many recent proposals to increase the number and frequency of space launches, in part due to the potential of future space markets. In this situation it is important to assess the impact of this new, larger launch market on the environment, both on Earth and in space (e.g. orbital debris).

In the space sector, there have been efforts to both characterise and mitigate environmental impacts of space activity, especially life-cycle assessments focusing on the ground segment and the space debris problem. The ESA Clean Space project is performing research in a number of these areas. One project in particular, EcoDesign, is developing comprehensive life-cycle assessment and design tools to account for the environmental impact of launch vehicles and spacecraft. This programme covers the entirety of space activity, from the production of components on satellites to the effect of launch vehicles during manufacturing and operation. Previous to these efforts, a series of studies on the environmental impact of launch vehicles on the stratosphere occurred, in-

*PhD student, robert.garner@strath.ac.uk
†PhD student, federico.toso@strath.ac.uk
‡Lecturer, christie.maddock@strath.ac.uk

cluding specific rockets such as the Delta II[2] and the Proton[3] rockets, with some detailed studies of the behaviour of plume dispersion and the afterburning[4] of species in the plume. These latter phenomenon can have major impacts on the emissions released.[5]

This paper presents an analysis and comparison of the H_2O emissions of a vertically-launched expendable rocket with a reusable spaceplane. The unique flight trajectory and novel hybrid propulsion systems, utilising liquid hydrogen and oxygen, used in SSTO spaceplanes are completely different to those used in the expendable launch vehicles of today. The Delta IV rocket was chosen as a test case as it has two variants that only use hydrogen and liquid oxygen as propellant, and their emissions can therefore be directly compared.

The trajectories of both a spaceplane and a Delta IV rocket are modelled. The former is constructed by optimising the trajectory using physical models for the dynamics, propulsion and aerodynamics. The latter by matching a dynamical model with publicly-available rocket flight data. The resultant emission profiles are compared, taking into the account their altitude distribution.

Multidisciplinary design and trajectory optimisation are useful tools for analysing the estimated performance of new vehicles, especially during the preliminary design phase. In particular, spaceplane trajectory design lends itself naturally to being constructed as a multiphase problem, decomposing the mission into flight segments, e.g., take-off, air-breathing mode in subsonic flight, supersonic flight, rocket mode in hypersonic flight, orbital insertion. Each phase of the trajectory can have different physical models, mission objectives, constraints and model fidelity level as necessary. The resultant program is modular and flexible and can be applied to a wide-range of trajectories, including ascent and descent. It also enables the user to investigate subsets of the trajectory, whilst optimising the cost function of the overall trajectory. The multiphase approach works especially well when there a number of discrete segments to the launch, such as staging or propulsion switches, in which there can be mathematical discontinuities in the models which cause problems for gradient-based solvers.

For this initial analysis, H_2O was chosen as the studied emitted species. Water is a greenhouse gas, but more importantly for the stratosphere, contributes to ozone depletion. In particular, H_2O in the stratosphere is a source of HO_2 radicals, and a catalyst for ice formation, both of which cause ozone depletion. Ross et al.[5] performed a series of studies on stratospheric ozone depletion, including the overall influence of the launch market. They highlight that launch vehicles are unique because they are the only source of anthropogenic chemical injection into the upper atmosphere, and in particular the lower stratosphere which is host to the ozone layer (altitude 20 - 30km). They also identified hypersonic propulsion systems as being of great interest, especially given earlier studies of the National Aero-Space Plane's impact on stratospheric ozone showing a reduction of 0.002 %/year[6] (for 200 annual flights) and potentially much more.[7] Both vehicles compared in this analysis use LH_2 (liquid hydrogen) and either atmospheric oxygen or onboard LOX (liquid oxygen) as propellants.

The spaceplane considered in this study is based upon the Hyperion vehicle proposed by Olds et al.[8] in the late 1990's. This was chosen as it is one of the few SSTO vehicle designs in open literature that also has validation against other models. The original design approach of the Hyperion vehicle was a multi-disciplinary integrated paradigm. Discipline specific models were coupled with each other, and were iterated over until a convergent solution was found. In particular, there was strong coupling between the propulsion, performance and sizing/mass models.

The rocket considered is the Delta IV M rocket. This was chosen because it is the only modern rocket in use that which only uses LH2 and LOX. Other versions of the Delta IV rocket are available, adding solid rocket boosters for most variants or additional LH2/LOX cores (Delta IV Heavy).

II VEHICLES AND SYSTEM MODELS

The vehicle designs used in the studies are the Hyperion spaceplane and the ULA Delta IV Medium rocket. The parameters of the Hyperion vehicle were taken directly from Olds et al.,[8] with the exception of the aerodynamics that were taken from a subsequent paper by Young et al.[9] which used the same vehicle to assess rail-launch SSTO vehicles.

The Hyperion vehicle is a single-stage-to-orbit vehicle with a conical forebody, highly swept wings and twin vertical winglets, shown in Fig. 2. It is powered by 5 LOX/LH2 ejector scramjet engines, which are capable of operating in four modes – ejector scramjet, ramjet, scramjet and rocket mode – enabling propulsion throughout every flight regime during an orbital ascent. The published payload mass[10] is 9072 kg to a 160 km altitude, circular orbit with an inclination

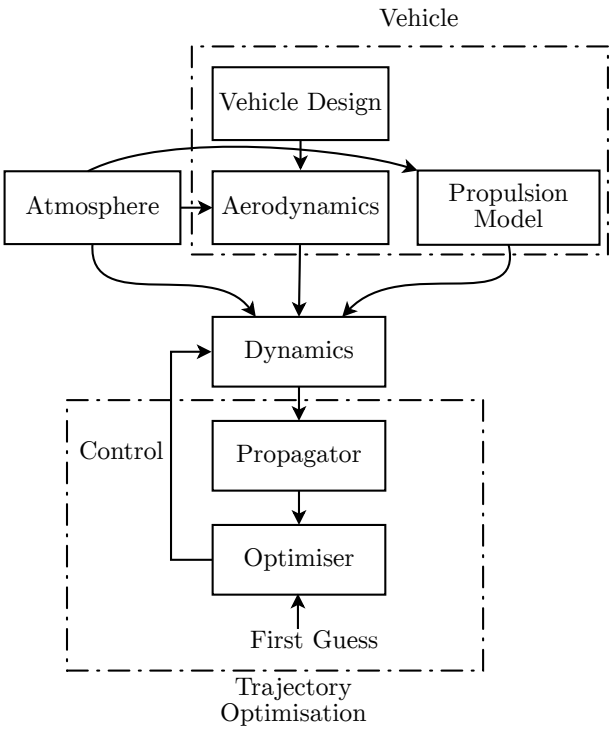

Fig. 1: Overview of the optimisation process

of 27.5°.

The Delta IV M is the smallest variant in the ULA Delta IV family of expendable launch vehicles (see Fig. 3). It is a single core vehicle, without boosters, which is powered by a RS-68A engine in the first stage, and an RL-10-B-2 engine in its upper stage. It is rated to deliver a 9190 kg payload to a 200 km altitude, circular orbit with an inclination of 28.5°.[11,12]

Table 1 displays the key mass parameters assumed in the study for both the spaceplane and the rocket. The published payload/orbit values by Olds et al. were generated assuming the trajectory followed a path of constant dynamic pressure and using an OMS to circularise the orbit. The trajectory used here for Hyperion was optimised using different system modelling software and an objective to minimise the required fuel mass onboard. Using the same gross take-off weight (GTOW) and dry mass, a substantially larger payload was found, 24254 kg compared to 9072 kg, that could be delivered to the same orbit as the Delta IV.

II.I Propulsion

This section describes the details of the modelling approaches for the propulsion system including emissions of both the spaceplane and the Delta IV.

	Hyperion (Olds et al.)	Hyperion (optimised)	Delta IV
Dry mass	61 439	61 439	30 780
Payload	24 254	9072*	9190
Propellant	277 498	292 680	224 401
Total Mass	363 191 kg	363 191 kg	292 680 kg

*Rated to a different orbit: 160 km LEO at $i = 27.5°$

Table 1: Mass budget of test vehicles to a 200 km LEO at 28.5° inclination

II.I.1 Spaceplane

The propulsion system of the Hyperion vehicle is a rocket-based combined cycle (RBCC) ejector-scramjet engine that combines rocket elements with air-breathing elements in a single unit. The propulsion system considered is a LOX/LH2 ejector scramjet system that is capable of operating in several modes: an rocket with ejector mode for low altitudes and velocities, high efficiency air-breathing ramjet and scramjet modes and as a rocket for higher altitudes and velocities. The average I_{sp} of the resulting propulsion combination is higher than that of a traditional expendable launch system, and enables the vehicle to be a single-stage-to-orbit vehicle.

The tool used to model this engine, HyPro, was developed and validated at Strathclyde by Mogavero.[13–15] HyPro was developed as a fast and modular software package for modelling combined-cycle propulsion systems for configurational engine optimisation, multi-disciplinary design optimisation and system analyses. It uses a 'jump solver' approach, where an engine is divided into components, and the analysis jumps in steps between the beginning of each component to the end. The choice of this method lends HyPro the flexibility to be able to model complicated and variable engine configurations. Other examples of propulsion codes that use this technique are the Ramjet Performance Analysis Code (RJPA) and SCCREAM[16] from Georgia Institute of Technology. EcosimPro, and its propulsion implementation ESPSS[17] use a similar approach, albeit solving the models simultaneously instead of sequentially.

Each component is bounded by a start and an end node, which represent the thermo-kinetic state at that position. The state at the end of the node is calculated based upon the first node and the equations that have been applied to the component.

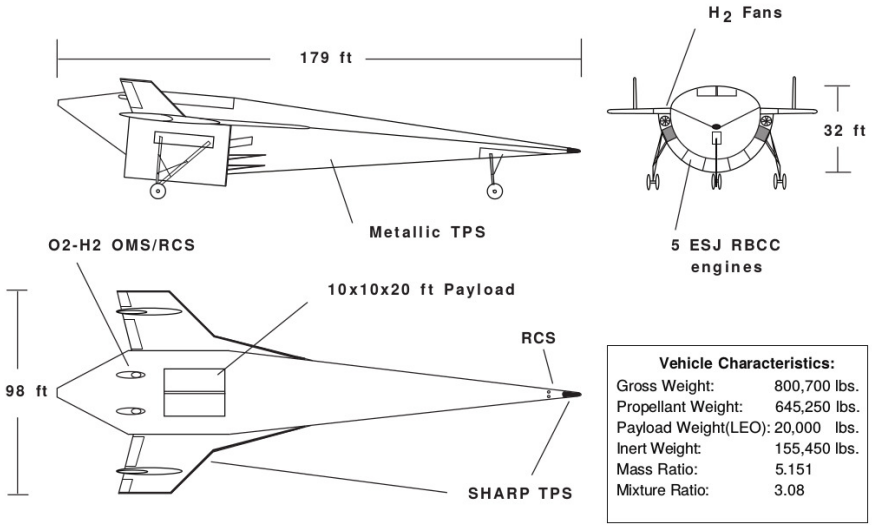

Fig. 2: Configuration of Hyperion Vehicle[10]

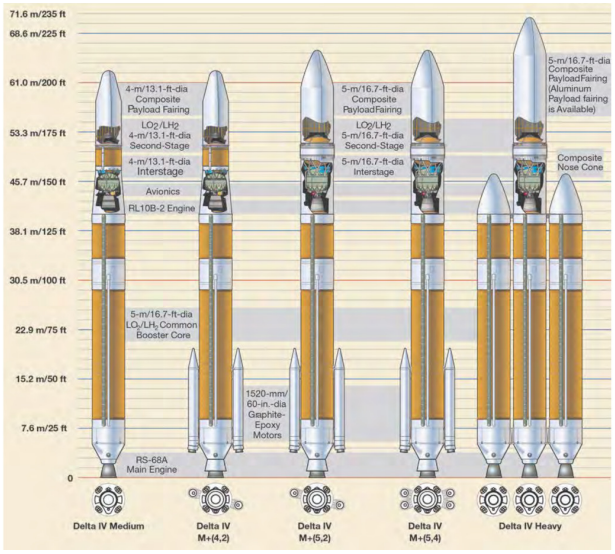

Fig. 3: Configuration of the Delta IV family[11]

HyPro was used to construct a surrogate model using the MATLAB curve-fitting tool for each propulsion system as a function of altitude and Mach number. This was done to increase the computational speed of the propulsion model, whilst maintaining an acceptable level of accuracy. The ramjet was fit with a (4,4) order bivariate polynomial, with a root-mean-squared-error of 6.95×10^4 N and maximum error of 4×10^5 N. Similarly, the scramjet and the rocket were fit with (4,2) order polynomials, with mean-squared-errors of 1.895×10^4 N and 833.7 N and maximum errors of 1.9×10^4 N and 6544 N respectively. A throttle, τ is applied directly to the resultant mass flow rate and thrust level of the engine,

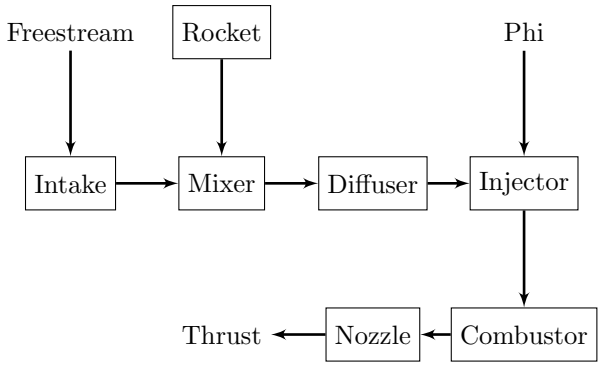

Fig. 4: Hyperion engine architecture

$$F_T = \tau F_{T(surrogate)} \quad [1a]$$

$$\dot{m} = \tau \dot{m}_{(surrogate)}. \quad [1b]$$

II.I.2 Delta IV

The propulsion system for Delta IV rocket was modelled using a standard rocket equation model. The first stage utilises a RS-68A LH_2/LOX rocket engine, and the second stage uses a RL10-B-2 LH_2/LOx engine. The parameters of these engines used in this study are shown in Table 2.

A reduction of thrust due to the atmospheric pressure is applied to maximum first stage thrust in a

Parameter	RS-68A	RL-10-B-2
Vacuum thrust	3560 kN	110 kN
Vacuum ISP	414 s	465.5 s
Mixture ratio	5.97	5.89

Table 2: Parameters of the Delta IV propulsion systems

vacuum,

$$F_{T,p} = F_{T,v} - A_e p(h) \quad [2]$$

where $p(h)$ is the pressure at the current altitude, $F_{T,v}$ is the vacuum thrust, $F_{T,h}$ is the thrust at the current altitude and A_e is the exit area of the nozzle.

II.I.3 Emissions Models

The H_2O emissions released by both vehicles are calculated based upon the mass flow rate at every time step of the integration. Since both vehicles use H_2 and O_2 propellent, the chemical equation governing the mass of H_2O produced is:

$$2\,H_2 + O_2 \longrightarrow 2\,H_2O \quad [3]$$

II.II Aerodynamics

The lift and drag forces are determined using the coefficients of lift and drag and a single reference area for the vehicle.

$$L = \frac{c_L \rho v^2 S_{ref}}{2} \quad [4a]$$

$$D = \frac{c_D \rho v^2 S_{ref}}{2} \quad [4b]$$

centered where ρ is the atmospheric density, v is the vehicle velocity, and S_{ref} is the vehicle reference surface area.

II.II.1 Spaceplane

The aerodynamics of the spaceplane are modelled by calculating the coefficients of drag, c_D and lift c_L as a function of the Mach number M and angle of attack α of the vehicle. The curves for the the c_D and c_L are taken from Young et al.[9] who further developed the Hyperion concept to create a secondary vehicle Lazarus. The mission profile of the vehicle was altered by using a sled-launch system, but the overall vehicle design was kept the same. The aerodynamics were calculated using the CBAERO software package and are shown in Fig. 5.

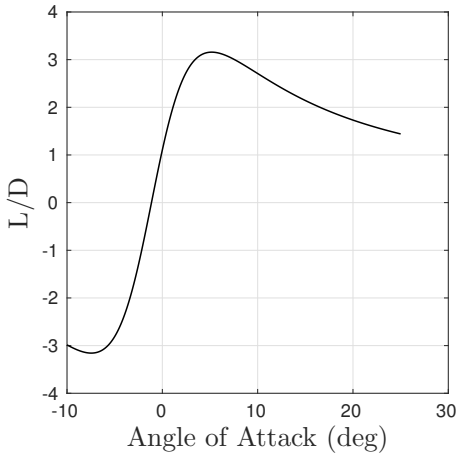

(a) Lift-to-Drag ratio as a function of the angle of attack

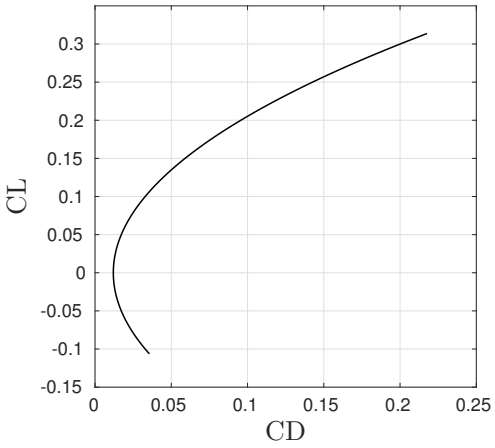

(b) Coefficient of lift against coefficient of drag

Fig. 5: Aerodynamic properties used in the spaceplane trajectory optimisation[9]

II.II.2 Rocket

The aerodynamics of the rocket are modelled by neglecting the lift component and calculating the drag assuming a constant $C_D = 1$, which is likely much higher than reality.[18] However, the difference between the angle of attack and the flight path is always zero in this model, i.e. the S_ref is always the cross-sectional area of the rocket, so there is an additional drag component not accounted for here.

II.III Operating Environment

The atmospheric model used was the International Standard Atmosphere. This provides the atmospheric pressure p and temperature at particular alti-

tude, h. From these the air density ρ and local speed of sound are calculated. This model divides the atmosphere into layers, each has a linear temperature distribution with altitude. Both the pressure and the density are found by solving the vertical pressure variation and the ideal gas law.

The Earth is modelled as a spherical, rotating planet with radius $R_E = 5\,375\,253\,\mathrm{m}$ and an angular velocity of $\omega_E = 7.292\,115 \times 10^{-5}\,\mathrm{rad\,s^{-1}}$. The Earth's acceleration due to gravity is modelled as a function of altitude,

$$g = \frac{\mu_E}{r^2} = \frac{\mu_E}{(h + R_E)^2} \quad [5]$$

where the standard gravitational parameter, $\mu_E = 398\,600.4418\,\mathrm{km^3\,s^{-2}}$.

II.IV Flight dynamics and control

Both vehicles are considered to be a point with variable mass, centred at the centre of mass of the vehicle. The vehicle is flying around a spherical, rotating Earth and the dynamics are therefore formulated with respect to a geocentric rotating reference frame using spherical coordinates.

The state vector of the vehicle is $\mathbf{x} = [h, \lambda, \theta, v, \gamma, \chi]$ where h is the altitude, v is the velocity in the Earth-centred Earth-fixed reference frame, γ is the flight path angle, χ is the heading, λ is the latitude, θ is the longitude. The equations of motion are:[19]

$$\dot{h} = \dot{r} = v \sin\gamma \quad [6a]$$

$$\dot{\lambda} = \frac{v \cos\gamma \sin\chi}{r} \quad [6b]$$

$$\dot{\theta} = \frac{v \cos\gamma \cos\chi}{r \cos\lambda} \quad [6c]$$

$$\dot{v} = \frac{F_T \cos(\alpha) - D}{m} - g \sin\gamma + \omega_e^2 r \cos\lambda \left(\sin\gamma \cos\lambda - \cos\gamma \sin\chi \sin\lambda\right) \quad [6d]$$

$$\dot{\gamma} = \frac{F_T \sin(\alpha) + L}{mv} \cos\mu - \left(\frac{g}{v} - \frac{v}{r}\right) \cos\gamma + 2\omega_{\mathrm{E}} \cos\chi \cos\lambda + \omega_{\mathrm{E}}^2 \left(\frac{r}{v}\right) \cos\lambda \left(\sin\chi \sin\gamma \sin\lambda + \cos\gamma \cos\lambda\right) \quad [6e]$$

$$\dot{\chi} = \frac{L}{mv \cos\gamma} \sin\mu - \left(\frac{v}{r}\right) \cos\gamma \cos\chi \tan\lambda + 2\omega_{\mathrm{E}} \left(\sin\chi \cos\lambda \tan\gamma - \sin\lambda\right) - \omega_{\mathrm{E}}^2 \left(\frac{r}{v \cos\gamma}\right) \cos\lambda \sin\gamma \cos\chi \quad [6f]$$

where m is the mass of the vehicle, F_T is the magnitude of the thrust from the engine, L and D are the lift and drag of the aerodynamic forces on the vehicle, $r = R_E + h$ where R_E is the Earth's radius, ω_E is the rotational velocity of the Earth, g is the acceleration due to gravity. The flight path angle γ is defined as being the angle between the local horizon and the velocity vector, and the flight heading angle χ is defined as the angle between north and the horizontal component of the velocity vector. The control law governs the angle of attack α, bank angle μ and the propulsion throttle of the vehicle.

III TRAJECTORY OPTIMISATION

The trajectory is determined using an in-house Spaceplane Integrated Design Environment software.[20–22] The approach uses flight segment decomposition technique with direct, multi-shooting transcription and solved with a local optimiser based on sequential quadratic programming and/or interior point methods.

The flight phase decomposition approach allows the user to define any number of mission phases. Within each phase, the number of shooting elements, control nodes, system models, integration and interpolation methods can all be specified. This allows for greater flexibility in configuring the problem, but does require knowledge of the system by the user. Discontinuities in the state and control variables are allowed by the system based on the matching conditions defined between each phase.

III.I Optimal Control

The optimal control problem is transcribed into an nonlinear programming (NLP) problem by using a multi-phase, multiple-shooting approach. The mission is initially divided into n_p user-defined phases. Within each phase, the time interval is further divided into n multiple shooting segments.

$$\cup_{k=1}^{n_p} \cup_{i=0}^{n-1} [t_{i,k}, t_{i+1,k}] \quad [7]$$

With each interval $[t_{i,k}, t_{i+1,k}]$, the control is further discretised into n_c control nodes $\{u_0^{i,k}, ..., u_{n_c}^{i,k}\}$ and collocated on Tchebycheff points in time.

Continuity constraints on the control and states are imposed,

$$\left.\begin{array}{l} \mathbf{x}_{i,k} = F([t_{i-1,k}, t_{i,k}], \mathbf{x}_{i-1,k}) \\ \mathbf{u}_{n_c}^{i-1,k} = \mathbf{u}_0^{i,k} \end{array}\right\} \text{ for } k = 1, ..., n_p \quad [8]$$

$$\left.\begin{array}{l} \mathbf{x}_{1,k} = \mathbf{x}(t_{n+1,k-1}) \\ \mathbf{u}_0^{1,k} = \mathbf{u}_{n_c}^{n+1,k-1} \end{array}\right\} \text{ for } k = 2, ..., n_p \quad [9]$$

where $F([t_{i-1,k}, t_{i,k}], \mathbf{x}_{i-1,k})$ is the final state of the numerical integration on the interval $[t_{i-1,k}, t_{i,k}]$ with initial conditions $\mathbf{x}_{i-1,k}$. This approach increases the degree of freedom of the optimisation process reducing the sensitivity of the overall problem to its variables although at a cost of a steep increase in the number of optimisation variables.

The optimisation variables are therefore:

- The initial state vector of each shooting segment within every phase (excluding the first segment of the first phase) $\mathbf{x}_{i,k}$
- The control nodes of each shooting segment $\{\mathbf{u}_0^{i,k}, ..., \mathbf{u}_{n_c}^{i,k}\}$
- The time of flight for each shooting segment $\Delta t_{i,k}$

The discretised optimisation problem is defined as

$$\min_{\{\mathbf{u}_j^{i,k}\},\{\mathbf{x}_{i,k}\},\{\Delta t_{i,k}\}} \phi(\mathbf{x}_{n,n_p}) + \sum_{k=1}^{n_p}\sum_{i=0}^{n-1} \Delta t_{i,k} f_0(\mathbf{x}_{i,k}, \mathbf{u}_j^{i,k}) \quad [10]$$

subject to

$$\begin{aligned} \mathbf{x}_{i,k} &= F([t_{i-1,k}, t_{i,k}], \mathbf{x}_{i-1,k}), \\ \mathbf{u}_{n_c}^{i-1,k} &= \mathbf{u}_0^{i,k}, \\ \mathbf{x}_{1,k} &= \mathbf{x}(t_{n+1,k-1}), \\ \mathbf{u}_0^{1,k} &= \mathbf{u}_{n_c}^{n+1,k-1}, \\ c(x(t), u(t)) &\leq 0, \quad t \in [t_0, t_f] \\ g(\mathbf{x}_{n,k}, \mathbf{u}_{n_c}^{n,k}) &\leq 0, \\ \omega(\mathbf{x}_{0,1}, \mathbf{x}_{n,n_p}) &= 0 \end{aligned}$$

for $i = 1, ..., n-1$, $k = 1, ..., n_p$ and $\Delta t_{i,k} = t_{i+1,k} - t_{i,k}$. Path constraints are evaluated at a discrete set of points based in time, and $g(\mathbf{x}_{n,k}, \mathbf{u}_{n_c}^{n,k})$ are the inequality constraints for phase switching.

III.II Optimisation Algorithm

The NLP problem is solved using the local interior-point optimisation in MATLAB's `fmincon` function.

One of the major limitations of trajectory optimisation is the need to produce good first guesses of the trajectory. Both convergence and the optimality of the final solution are heavily dependent on the first guess. Both a user-input first guess control law, or a global-search optimisation can be used to generate this. The former could be previous trajectory data, an expected result or a designed solution (for example, taking into account the optimal regime of the propulsion system). Alternatively, the user could input a constant control law. The second method is to use a stochastic global search to quickly survey the entire survey space. A constant control law was chosen as the first guess for all optimisations in this paper.

IV TEST CASE

IV.I Spaceplane

The test case chosen was a mission to launch a payload to 28.5° 200 km orbit, as if it were taking off from the Kennedy Space Center. The trajectory has three propulsion models applied, the ramjet, scramjet and rocket. The time, velocity and altitude at which switching between them occurs has not been constrained. The control parameters for the ascent trajectory are $\mathbf{c} = [\alpha, \tau, t_{tof}]$, where t_tof is the time of flight of each phase. The control law is discrete, and characterised by a number nodes in each phase distributed using a Chebyshev distribution for each phase. The control is interpolated between these points using a Piecewise Cubic Hermite Interpolating Polynomial, written as a fast Matlab-generated MEX function.

The control space is constrained by the following bounds: $\alpha \in [-10°, 30°]$ and $\tau \in [0.8, 1]$ for the ramjet and scramjet phases, and $\tau \in [0.6, 1]$ for the rocket phases. There are five phases in total, two each for the ramjet and scramjet propulsion systems, and one for the rocket phase. The ramjet and scramjet phases each have 4 control nodes, and the rocket phase has 10 control nodes. The time is constrained to a maximum of 300 s for the ramjet and scramjet phases, and 500 s for the rocket phase.

The initial parameters for the state vector are:

$$\begin{aligned} h(t=0) &= 8\,\text{km} \\ v(t=0) &= 900\,\text{m}\,\text{s}^{-1} \\ \gamma(t=0) = \lambda(t=0) &= \chi(t=0) = 0° \\ \phi(t=0) &= 27.5° \\ m(t=0) &= 325\,000\,\text{kg} \end{aligned} \quad [11]$$

where the altitude, velocity and mass are calculated based upon the flight profile Hyperion. There are no constraints applied to phases, and therefore the time at which the vehicle switches will purely be a function of the models.

The objective of the optimisation is to maximise the payload mass to orbit. That is, for a fixed vehicle mass, and a known maximum wet mass, the two free mass variables are the mass of the on-board propellant and the payload mass into orbit. Therefore, the

objective function is

$$\min_{c \in D} m_p(t = t_f). \quad [12]$$

Additional constraints are placed on the maximum vehicle acceleration in both the longitudinal and normal axis of the vehicle of $a_x, a_z \leq 3g_0\,\mathrm{m\,s^{-2}}$ and on the maximum dynamic pressure of the vehicle during flight $q = \frac{1}{2}\rho v^2 \leq 300\,000\,\mathrm{Pa}$.

IV.II Delta IV

The Delta IV trajectory was reconstructed by propagating over a trajectory using the vehicle and system models described in section II. MATLAB's `ode45` integrator, which is based on an explicit Runge-Kutta (4,5) formula, the Dormand-Prince pair was used for this. A time-based control law was applied for the flight path angle, γ of the rocket during flight, The throttle, τ was assumed to be 1 unless the rocket exceeded an acceleration limit, when the throttle would be reduced. This acceleration limit was based on the acceleration environment described in the Delta IV User Manual. The rate of change of the flight path angle was adjusted until the resultant trajectory matched the known trajectory points of the vehicle described in the ULA Users Manual. As this study is investigating the altitude distribution of emissions, the most important parameter curves to match were the altitude vs. time/downrange profiles, and the mass to orbit.

IV.III Results

The result of the trajectory optimisation for the spaceplane is a trajectory that achieves the requested orbited and all other constraints - and has a final burnout mass of 85 692 kg, including the payload mass. This results in a payload mass of around 24 254 kg, over twice that of the reference Hyperion vehicle given in Olds et al. There are a number of possible reasons for the discrepancy. There are uncertainties in the models used within this simulation, as well as those in the reference papers. HyPro in particular predicts higher thrusts and specific impulses compared with the SCCREAM solver, although Mogavero suggests that HyPro matches other data sources.[15] Perhaps the most likely reason is that the trajectory presented here is an optimal solution, although probably not the global solution. The trajectory produced by Olds was assumed to be flying along the propulsion-optimal constant dynamic pressure trajectory, and is unlikely to be vehicle-optimal for this reason.

The key flight parameters are shown in figs. 6 to 9, and the trajectory is combined with emissions data in fig. 10. Figure 6 shows the flight path angle of the trajectory, and the angle of attack used to produce this trajectory, which stays within the bounds. The thrust curve in fig. 8 shows how the thrust varies with time through the flight. The throttle can be disconnected between phases, which is why the thrust isn't continuous and connected. One of the constraints that was applied to this optimisation was the dynamic pressure, at 2×10^5 Pa, whereas Hyperion flew on a 95 760 Pa dynamic pressure boundary. The ramjet has an operational range of $2.5 \leq M \leq 6$ whilst the scramjet has an operational range of $5 \leq M \leq 10$. The point at which the vehicle switched propulsion systems is chosen by the optimiser, in this case the vehicle switched from ramjet to scramjet at mach 5.7, and from scramjet to rocket at mach 9.8.

Figure 10 shows a direct comparison between the Delta IV and the spaceplane. Both the trajectory (altitude vs. time) and the mass flow rate of H_2O with time are plotted. The H_2O released by the spaceplane is much higher than that of the Delta IV, since the propellant carried on board the spaceplane for the air-breathing phase is all hydrogen. For the spaceplane, 5.0143×10^5 kg of H_2O was generated along the trajectory, and 2.24×10^5 kg by the Delta IV. The amount H_2O produced by its first propulsion system, the ejector, hasn't been included in this total, so the amount produced by the spaceplane is significantly higher. Figure 11 shows the altitude distribution over which this H_2O was released. The altitude region in which the emitted H_2O peaks is between 20 - 30 km, the area of the lower stratosphere where the ozone layer exists. The Delta IV on the other hand does not spend much time in this region of the atmosphere, as it is still under power from the first stage, and a large amount of its time of flight is spent at altitude increasing its velocity to orbital velocity.

V CONCLUSIONS

This paper has outlined an approach for investigating the emissions of transatmospheric vehicles, in this case an expendable launch vehicle and a spaceplane concept. The scenario explored investigates the environmental impact of an ascent trajectory of both of these vehicles to a 200 km 27.5° orbit. The results show that higher amounts of H_2O are dispersed into the atmosphere from the spaceplane than the Delta IV. Of particular concern is that the peak emissions for the spaceplane are within the lower stratosphere,

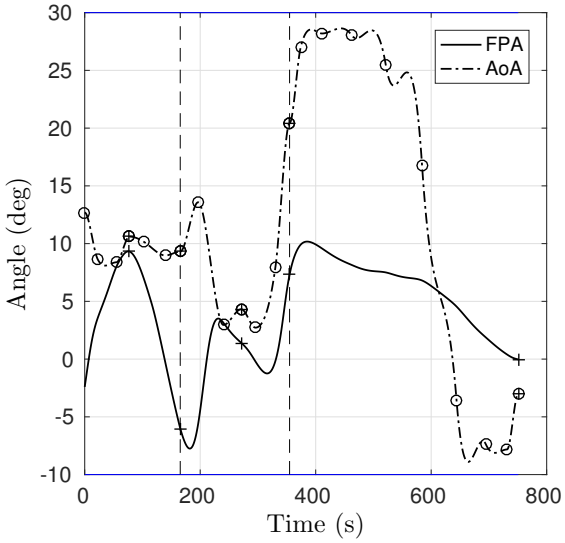

Fig. 6: Both the flight path angle and the angle of attack are plotted in this figure. The circles on the angle of attack line represent the control nodes from which the control law is interpolated. The dotted lines represent the propulsion switches.

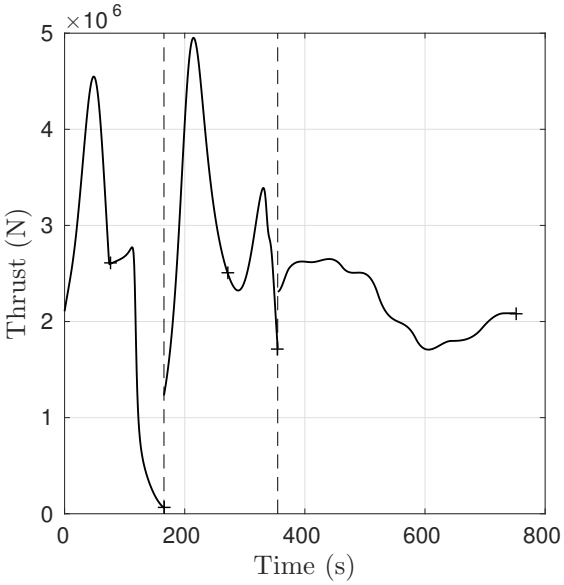

Fig. 8: The thrust of the Hyperion vehicle during the flight. The influence of this on the Mass Flow of H_2O is apparent. Dotted line indicates the change in propulsion system.

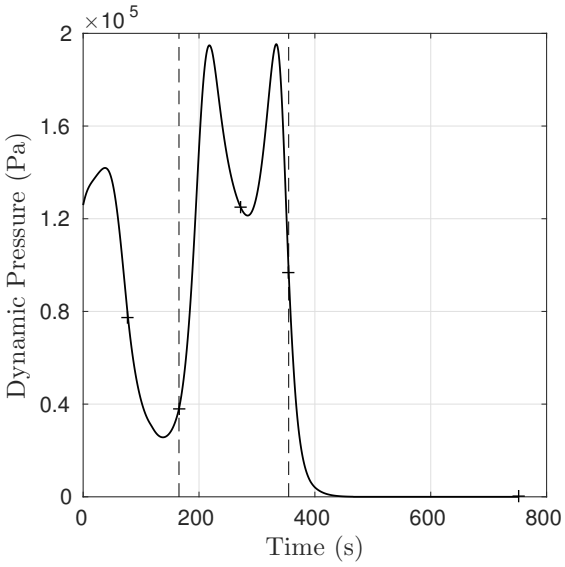

Fig. 7: Dynamic Pressure of the Hyperion spaceplane during the flight. A maximum constraint of 2×10^5 Pa was applied. Dotted line indicates the change in propulsion system.

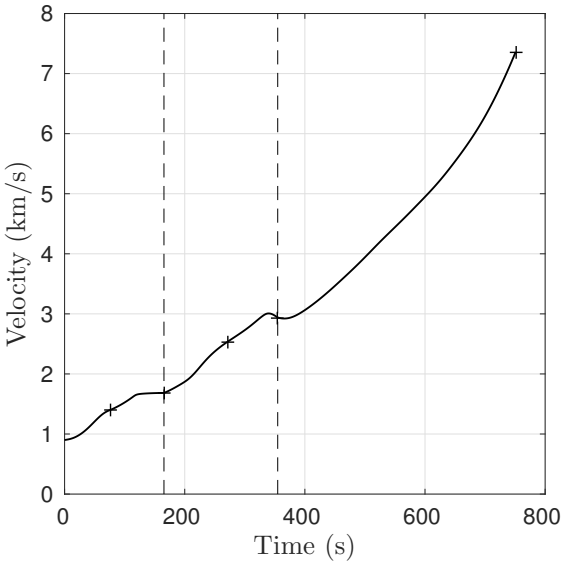

Fig. 9: The velocity of the Hyperion vehicle during the flight. The vehicle achieves the requested orbital velocity, and the propulsion systems switched in at the limits of their capability. Dotted lines indicate the propulsion system switch.

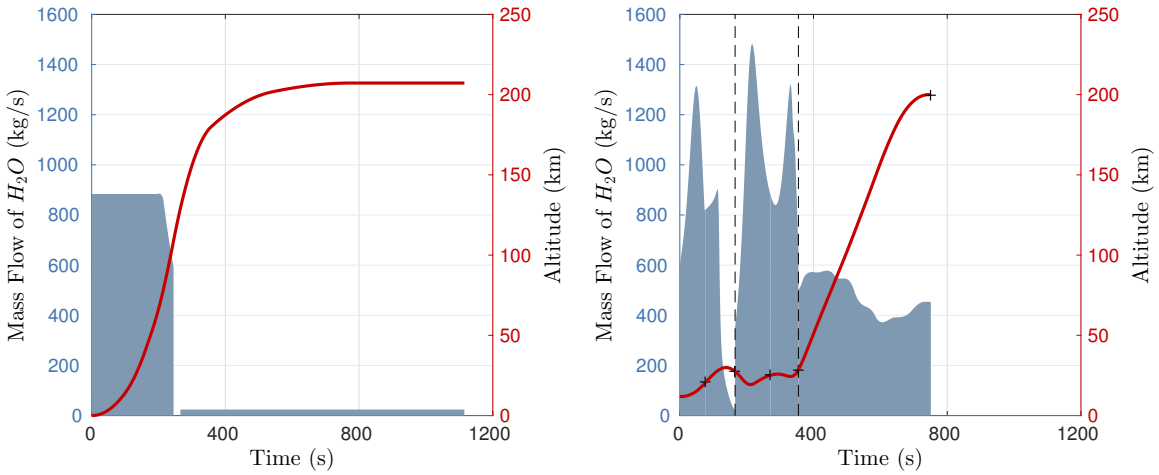

(a) Delta IV (b) Spaceplane

Fig. 10: Comparison of Delta IV and Spaceplane mass flow rate of H_2O emissions with time. The red line indicates the trajectory (altitude with time). The area highlighted in blue represents the total emissions from each launch vehicle.

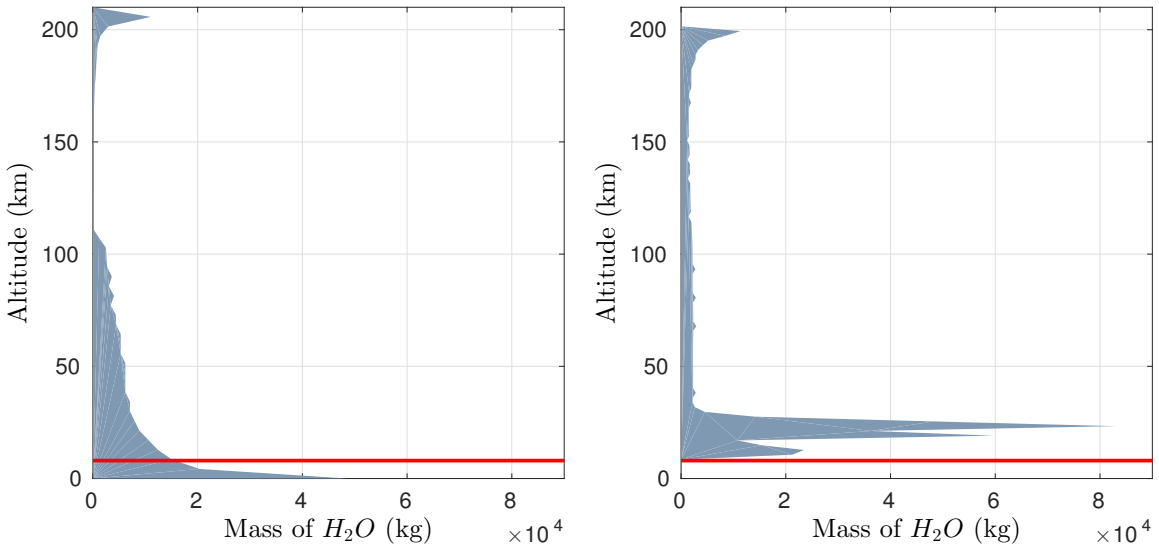

(a) Delta IV (b) Spaceplane

Fig. 11: Comparison of Delta IV and Spaceplane mass of H_2O emissions with altitude. The red line indicates the point at which the spaceplane trajectory is started. The data has been binned and plotted into altitude bins of 4km.

between 20 - 30km. At this altitude range H_2O can have a major impact on ozone depletion.

Future work could include improving the launch vehicle atmosphere interaction, by modelling important phenomena like the plume and combustion after the exhaust exit. This methodology can also be extended to cover other trajectories or vehicles, including point-to-point supersonic and hypersonic transportation and other launch vehicles. It can be further extended to investigate other emissions, such as NOx, CO_2, CO and SO_2 and propellant types such as kerosene, methane or solid propellants. It can also be integrated into a design platform for vehicle concepts, extending the multidisciplinary design process from solely performance and operational objectives to include environmental concerns.

REFERENCES

[1] Varvill, R. and Bond, A., "A Comparison of Propulsion Concepts for SSTO Reusable Launchers," *Journal of the British Interplanetary Society*, Vol. 56, 2003, pp. 108–117.

[2] Ross, M., Toohey, D., Rawlins, W., Richard, E., Kelly, K., Tuck, A., Proffitt, M., Hagen, D., Hopkins, A., Whitefield, P., et al., "Observation of stratospheric ozone depletion associated with Delta II rocket emissions," *Geophysical research letters*, Vol. 27, No. 15, 2000, pp. 2209–2212.

[3] Ross, M., Danilin, M., Weisenstein, D., and Ko, M. K., "Ozone depletion caused by NO and H2O emissions from hydrazine-fueled rockets," *Journal of Geophysical Research: Atmospheres*, Vol. 109, No. D21, 2004.

[4] Brady, B., Martin, L., and Lang, V., "Effects of launch vehicle emissions in the stratosphere," *Journal of spacecraft and rockets*, Vol. 34, No. 6, 1997, pp. 774–779.

[5] Ross, M., Toohey, D., Peinemann, M., and Ross, P., "Limits on the space launch market related to stratospheric ozone depletion," *Astropolitics*, Vol. 7, No. 1, 2009, pp. 50–82.

[6] Liu, S. K., *Aerospace-Plane Flights and Stratospheric Ozone: Review and Preliminary Assessment of the National Aerospace Plane (NASP) Operations*, Vol. 3464, Rand Corporation, 1992.

[7] Grooß, J.-u., Brühl, C., and Peter, T., "Impact of aircraft emissions on tropospheric and stratospheric ozone. Part I: Chemistry and 2-D model results," *Atmospheric Environment*, Vol. 32, No. 18, 1998, pp. 3173–3184.

[8] Olds, J. R. and Bradford, J., "SCCREAM (Simulated Combined-Cycle Rocket Engine Analysis Module): A conceptual RBCC engine design tool," *Joint Propulsion Conference*, 1997.

[9] Young, D. A., Kokan, T., Clark, I., Tanner, C., and Wilhite, A., "Lazarus: A SSTO Hypersonic Vehicle Concept Utilizing RBCC and HEDM Propulsion Technologies," *International Space Planes and Hypersonic Systems and Technologies Conference*, AIAA, 2006.

[10] Olds, J., Bradford, J., Charania, A., Ledsinger, L., McCormick, D., and Sorensen, K., "Hyperion: an SSTO vision vehicle concept utilizing rocket-based combined cycle propulsion," *AIAA paper*, 1999, pp. 99–4944.

[11] ULA, "Delta IV Launch Services Users Guide," Tech. rep., United Launch Alliance, 2013.

[12] "Space Launch Report - Delta IV," `http://www.spacelaunchreport.com/delta4.html`, Accessed: 2016-09-07.

[13] Mogavero, A. and Brown, R. E., "An improved engine analysis and optimisation tool for hypersonic combined cycle engines," *AIAA International Space Planes and Hypersonic Systems and Technologies Conference*, 2015.

[14] Mogavero, A., Taylor, I., and Brown, R. E., "Hybrid Propulsion Parametric and Modular Model: a novel engine analysis tool conceived for design optimization," *AIAA International Space Planes and Hypersonic Systems and Technologies Conference, Atlanta GA*, 2014, pp. 16–20.

[15] Mogavero, A., *Toward automated design of Combined Cycle Propulsion*, Ph.D. thesis, University of Strathclyde, 2016.

[16] Olds, J. R. and Bradford, J. E., "SCCREAM: a conceptual rocket-based combined-cycle engine performance analysis tool," *Journal of Propulsion and Power*, Vol. 17, No. 2, 2001, pp. 333–339.

[17] Villacé, V. F. and Paniagua, G., "Simulation of a Combined Cycle for High Speed Propulsion," 2010.

[18] Naughton, J. W., "Reduction of Base Drag on Launch Vehicles," 2002.

[19] Tewari, A., *Atmospheric and space flight dynamics*, Springer, 2007.

[20] Ricciardi L, Toso F, V. M. M. C., "Multi-objective optimal control of the ascent trajectories of launch vehicles," *Astrodynamics Specialist Conference, AIAA Space and Astronautics Forum and Exposition*, 2016.

[21] Toso, F., Maddock, C., and Minisci, E., "Optimisation of Ascent Trajectories for Lifting Body Space Access Vehicles," *Space transportation solutions and innovations symposium, International Astronautical Congress*, 2015.

[22] Pescetelli, F., Minisci, E., Maddock, C., Taylor, I., and Brown, R., "Ascent Trajectory Optimisation for a Single-Stage-to-Orbit Vehicle with Hybrid Propulsion," *AIAA/3AF International Space Planes and Hypersonic Systems and Technologies Conference*, 2012, p. 5828.